RSC Advances

REVIEW

View Article Online
View Journal | View Issue

Cite this: *RSC Adv.*, 2024, **14**, 32370

Green anti-solvent engineering for high-efficiency and environmentally friendly perovskite solar cells

Yuwen Yang, Zhaolong Huang, Hao Gao, * Zicong Xu, Weihong Fang, Yichuan Chen, Yuehui Hu, Zhijie Yi, Jiayu Huang and Hua Zhu

Flat and dense perovskite films with low defect density are essential for high-performance perovskite solar cells (PSCs). Anti-solvent-assisted crystallization (ASAC) is one of the effective ways to obtain high-quality perovskite films with low cost and simple operation. However, most of the traditional anti-solvents such as chlorobenzene, toluene, and diethyl ether have strong toxicity, which would be harmful to people's physical and mental health. It can be anticipated that when these toxic anti-solvents are widely applied in the industry, they will have destructive effects on humans and the environment, which is contrary to the current promotion concepts of green environmental protection. In September 2015, the United Nations Development Program regulated the Sustainable Development Goals (SDGs) for Mankind, which clearly emphasized the use of economically viable clean energy that was compatible with the goals for climate action, good health and well-being. So the development of non-hazardous green anti-solvents is an important direction in the research field of PSCs. In this review paper, the outstanding research achievements on green anti-solvents in recent years are summarized, including different types of perovskite films using different green anti-solvents with/without additives, the physical and chemical properties of different green anti-solvents, and their effects on the performance of perovskite films and PSCs. Moreover, five types of non-anti-solvent green preparation methods regulated by physical processes are also assessed. It provides references for the manufacturing of efficient, stable, low-cost and environmentally friendly perovskite devices.

Received 14th July 2024
Accepted 21st September 2024

DOI: 10.1039/d4ra05082g

rsc.li/rsc-advances

1 Introduction

The use of renewable energy has become particularly important amid the depleting fossil fuel resources and escalating environmental issues.[1,2] Solar energy, as a widely distributed and inexhaustible clean energy source, holds tremendous potential for exploitation. Moreover, PSCs possess excellent photoelectric properties, including a high extinction coefficient, long carrier diffusion length, high carrier mobility, high tolerance for defects, and controllable band gap, all coupled with a simple manufacturing process. Therefore, they are increasingly attracting the attention of researchers worldwide.[3,4] In the past decade or so, the energy conversion efficiency of PSCs has increased significantly, from an initial 3.8% to the current 26%,[5,6] reaching a level comparable to that of traditional crystalline silicon solar cells. As a result, they have become the most promising candidates for the third generation of organic photovoltaic cells with great application prospects. One of the biggest advantages of PSCs is their ability to be fabricated through a one-step film formation process. This preparation method is straightforward and easy to implement, leading to consistent film thickness and remarkable scalability.[7–9] However, the polycrystalline films processed by the traditional one-step method inevitably experience anisotropic growth as a result of the relatively slow evaporation of solvents, leading to a low nucleation density and poor coverage of the perovskite film. Consequently, this results in relatively low efficiency for the fabricated PSCs.[10,11] Therefore, researchers are striving to increase the nucleation density and coverage of perovskite films in order to effectively boost the energy conversion efficiency of the devices. Based on this, a series of methods have been developed to prepare high-quality perovskite films, such as the two-step method, the additive engineering method, the dual source co evaporation method and the hydrothermal method.[12,13] And the ASAC is an improvement upon the traditional one-step method. Because of its simplicity in processing, wide range of applicability, high separation efficiency, and effective elimination of the primary solvents DMF and DMSO, it has become one of the most widely used methods.[14–17] In this method, the role of the anti-solvent is to enhance the solute concentration by accelerating the evaporation of the solvent during the preparation process through adjusting the solvent concentration, solvent polarity, and controlling the rate of solvent evaporation. This initiates nucleation and crystallization, which in turn passivates defects and results in the

School of Mechanical and Electronic Engineering, Jingdezhen Ceramic University, Jiangxi 333403, China

Table 1 Basic properties of anti-solvents

Toxicity	Anti-solvent name	Fundamental properties	Boiling point	Chemical polarity
Highly toxic	Chlorobenzene (CB)	Colorless transparent liquid, bitter almond flavor, long term contact is prohibited, both steam and liquid are toxic	132.2 °C	High polarity
	Toluene (TL)	Colorless transparent liquid, with a unique aromatic aroma, steam is toxic and can cause harm to the human body through the respiratory tract	111 °C	Low polarity
	Ethyl ether (DE)	Colorless transparent liquid, aromatic aroma, high acute toxicity, with anesthetic effects on the central nervous system	34.6 °C	Low polarity
Almost non-toxicity	*Sec*-butyl ethanol (2-BA)	Colorless and transparent liquid, with a wine like odor, biodegradable, organic solvent	99.5 °C	High polarity
	Ethanol	Flammable, volatile, colorless and transparent liquid (at room temperature and pressure), with a slight alcohol odor	78.3 °C	High polarity
	N-Propyl acetate (NPAC)	Colorless clear liquid with transparency, stable at room temperature, highly flammable	102 °C	High polarity
	Propylene glycol methyl ether (PM)	Excellent solubility in organic solvents, suitable volatilization rate	120 °C	Neutral polarity
	Acetic acid (HAc)	Colorless hygroscopic liquid with a freezing point of 16.7 °C (62 °F)	117.9 °C	High polarity
	Ethyl acetate (EA)	Colorless and transparent liquid, with a pungent odor at high concentrations, easily volatile, sensitive to air, capable of absorbing moisture	77.5 °C	Neutral polarity
	Diethyl carbonate (DEC)	A dicarbonate ester of ethanol, colorless and transparent liquid (at room temperature)	126.8 °C	Low polarity
Low toxicity	Acetylacetone (AA)	Organic solvent, colorless or slightly yellow transparent liquid, with ester odor, slightly soluble in water	140.4 °C	High polarity
	Methyl acetate (MA)	Colorless transparent liquid, fruity aroma, slightly spicy taste, liquid at room temperature and pressure	56.9 °C	High polarity
	Isopropanol (IPA)	Organic solvent, colorless and transparent liquid, with an odor similar to a mixture of ethanol and acetone, soluble in water	82.5 °C	Low polarity
	Methyl benzoate (MB)	Organic solvent, colorless transparent liquid, insoluble in water	198 °C	Low polarity
	Methoxybenzene (PhOMe)	Green organic solvent with aromatic odor, insoluble in water	153.8 °C	Low polarity
	Anisole (ANS)	A pleasant aromatic odor, colorless to pale yellow liquid, insoluble in water	154 °C	Low polarity

production of a uniform and compact perovskite film. However, the early developed ASAC methods typically employed traditional toxic solvents such as chlorobenzene (CB),[18–20] toluene (TL),[21,22] and ethyl ether (DE)[23,24] (outlined in Table 1). These substances exhibit high volatility, making them easily released into the atmosphere from pollution sources. Once in the atmosphere, they can participate in photochemical reactions, forming photochemical smog that negatively impacts air quality. When leaked into soil, they infiltrate and contaminate soil layers, disrupting soil structure and functionality. This contaminated soil may no longer be suitable for crop cultivation or supporting other biological activities. Furthermore, chlorobenzene can potentially interfere with the endocrine system, altering sex hormone levels and subsequently affecting the development and function of reproductive organs. Toluene is a potent irritant; eye contact can result in pain and blurred vision, while inhalation of toluene vapor may trigger respiratory system disorders such as chronic rhinitis and bronchitis. In cases of acute exposure to large amounts of ethyl ether, early symptoms like excitement, drowsiness, vomiting, paleness, bradycardia, hypothermia, and irregular breathing can occur, posing a serious threat to life in severe cases.

Under such circumstances, researchers were required to use glove boxes, fume hoods, gas masks, and other protective equipment to isolate themselves from the harmful effects.[25,26] If these toxic solvents are applied to industrial production, it could pose potential dangers to researchers and workers, and cause harm to the environment. This would run counter to the goals of economically viable clean energy, climate action, and good health and well-being outlined in the 17 SDGs set by the United Nations Development Programme, and it does not align with the requirements of sustainable development. Therefore, the search for novel green anti-solvents that do not produce environmental side effects to replace traditional toxic anti-

solvents has emerged as a critical focus within this research area.[27–29] At the same time, many scientists are also committed to finding other green preparation methods of perovskite films without anti-solvents.

2 Green anti-solvent

Generally, solvents that have lower hazards and risks to the environment, human health, and sustainable development during their use process from synthesis to application, and then to treatment and recycling in various stages are called green solvents. They are called green anti-solvents when used in the preparation of perovskite thin films by ASAC method. The spin-coating process of the perovskite precursor solution employs an anti-solvent treatment in order to efficiently remove the main solvent and trigger the crystallization of the perovskite film. The preparation method utilizing ASAC can be simplified into a model, in which the application of the anti-solvent initiates two distinct processes. By adding a liquid anti-solvent onto the surface of the diluted precursor solution, the bulk solvents DMF and DMSO are extracted from the underlying layer through the process of diffusion. Throughout this period, a constant supply of pure anti-solvent is maintained on the precursor layer, ensuring a high diffusion gradient and maximizing the efficiency of the process. Concurrently, the extraction of solvents from the precursor solution triggers nucleation and crystallization of the perovskite material, ultimately leading to the formation of a polycrystalline film.[30]

In recent years, researchers have devoted significant efforts to developing green anti-solvents or other green preparation processes for perovskite thin films. By examining the effects of green anti-solvents on the quality, absorbance, and device performance of perovskite films, numerous meaningful research outcomes have been achieved.[31–35] Drawing upon the presentations of research accomplishments, we have summarized the fundamental properties of these anti-solvents (outlined in Table 1, chemical structures showed in Fig. 1), which display characteristics of elevated boiling points, and either complete non-toxicity or low toxicity. Furthermore, we comprehensively delineated the environmentally friendly processes of fabricating perovskite films and elaborated the impacts of various green anti-solvents on the morphology and performance of perovskite films, showcasing the vast prospects and sustainability of green anti-solvent-based PSCs production (Fig. 1).

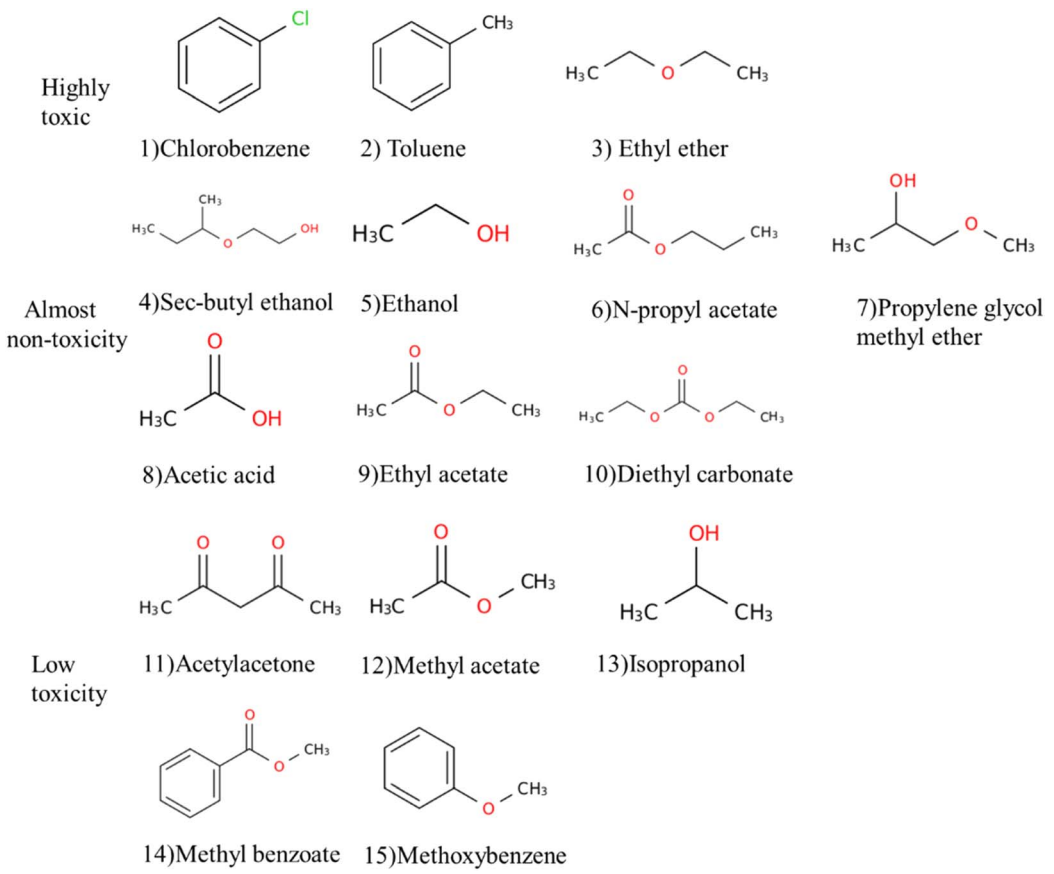

Fig. 1 According to the results in Table 1, the chemical structures of various anti-solvents used in perovskite films are divided into three categories: highly toxic (1) chlorobenzene, (2) toluene, (3) ethyl ether; almost non-toxic (4) *sec*-butyl ethanol, (5) ethanol, (6) *N*-propyl acetate, (7) propylene glycol methyl ether, (8) acetic acid, (9) ethyl acetate, (10) diethyl carbonate; low-toxic (11) acetylacetone, (12) methyl acetate, (13) isopropanol, (14) methyl benzoate, (15) methoxybenzene.

3 Preparation of perovskite films by green anti-solvent

As is widely known, ASAC serves as an efficient means to achieve dense and uniform perovskite films. This technique, characterized by its low cost and straightforward operation, currently stands as one of the most widely utilized methods for obtaining high-quality perovskite films. Initially, scientists often resorted to traditional anti-solvents such as CB, TL, and DE. While the PCE of PSCs fabricated using these anti-solvents was decent, they exhibited significant toxicity, rendering them unfriendly to both human health and the environment. Guided by the United Nations' sustainable development principles, scientists embarked on the investigation of green anti-solvents and made notable progress. Nevertheless, they simultaneously discovered that the PCE of the PSCs fabricated using these solvents fell short of that achieved with traditional toxic anti-solvents. When used in combination with precursor solution, these anti-solvents remove a large amount of organic halides, disrupting the microstructure of the films and leaving behind PbI_2 that could not be converted into perovskite, ultimately leading to irreversible changes in stoichiometry. Subsequently, researchers embarked on enhancing the performance by incorporating additives that can effectively passivate the Pb^{2+} coordination defects within the green anti-solvents. This article offers a comprehensive review of the noteworthy achievements made in the field of green anti-solvent research.

3.1 Preparation of green anti-solvent for $CH_3NH_3PbI_3$ perovskite films

$CH_3NH_3PbI_3$ perovskite is classified as a direct bandgap semiconductor, boasting a bandgap of roughly 1.55 eV. The positioning of its valence band and conduction band enables it to effectively inject electrons into the electron transport layer, while simultaneously possessing the necessary energy to inject excited holes into the hole transport layer. Moreover, $CH_3NH_3PbI_3$ perovskite boasts a significantly longer carrier diffusion length and lifetime, surpassing other organic semiconductor materials by 1–2 orders of magnitude. Additionally, it exhibits excellent thermal stability. These attributes contribute to the high electron mobility of $CH_3NH_3PbI_3$ perovskite and its exceptional performance in hole transport, enabling efficient operation in solar cells. Furthermore, the light absorption coefficient of $CH_3NH_3PbI_3$ perovskite is significantly high, exceeding that of ordinary organic dyes by more than 10 times, demonstrating its exceptional light absorption capability.

3.1.1 $CH_3NH_3PbI_3$ perovskite films with ethyl acetate (EA). (a) EA serving as a prototypical green anti-solvent, exhibits a notably high polarity of 0.228 and a considerably lower boiling point of 77.5 °C compared to other halogenated anti-solvents. Consequently, it facilitates the rapid crystallization of perovskite. The utilization of EA as an anti-solvent not only enhances the interfacial contact between functional layers and the stability of the perovskite film, but also facilitates the controlled growth of the perovskite crystals, resulting in a slower growth rate, high crystallinity, and dense microstructure. Consequently, high-quality perovskite with preferential crystal orientation, low-density trap states, and reduced charge recombination is achieved, as depicted in Fig. 2. The carbonyl group (C=O) present in EA exhibits electron-rich properties, facilitating the formation of hydrogen bonds with dimethyl sulfoxide. The hydrogen bonding interaction between the anti-solvent EA and dimethyl sulfoxide effectively inhibits the rapid evaporation of EA, subsequently slowing down the

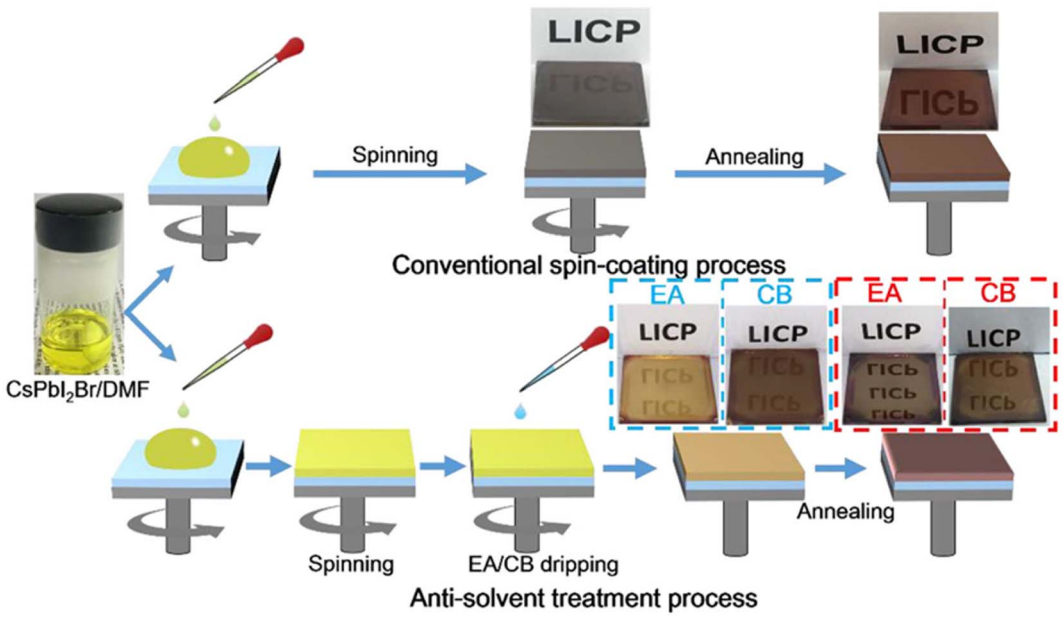

Fig. 2 Schematic diagram of traditional spin coating and anti-solvent treatment processes for manufacturing perovskite thin films (using EA and CB). This figure has been reproduced from ref. 36 with permission from Wiley, copyright 2018.

crystallization process of the $CH_3NH_3PbI_3$ layer. The fabricated $CH_3NH_3PbI_3$ PSCs have achieved a remarkable PCE of 17.75%, and remarkably, even the unencapsulated version of the cell demonstrates excellent long-term and thermal stability.[37]

In comparison to the pure EA anti-solvent, the combined utilization of EA with an additive anti-solvent profoundly enhances the surface morphology of the perovskite film. This blend effectively passivates grain boundary/surface defects within the perovskite film, thereby markedly boosting both the photovoltaic performance and reproducibility of the device. The following serves as an illustrative example of the preparation of $CH_3NH_3PbI_3$ perovskite films through the utilization of EA as an anti-solvent in conjunction with various additives.

(b) After undergoing several initial steps, intermediate phases emerge at the surface and grain boundaries of the perovskite. These intermediates are thoroughly extracted *via* robust hydrogen bonding interactions with the EA solution. The overall configuration of the open grain boundaries enhances the contact between the entire perovskite particle and the hole-transporting material, facilitating faster charge separation at the interface. As a result of the continuous post-treatment process, surface defect states are reduced, leading to a notable improvement in electron transport. The sequentially processed PSCs demonstrate an impressive PCE of 18.46%, with an average steady-state PCE of 18.05%. Additionally, the reproducibility and stability of the devices have been significantly enhanced.[38]

(c) Treating perovskite with the combination of the anti-solvent EA and the additive acetylacetone (AA) enables fine-tuning of the crystallization process and defect reduction, ultimately yielding a $CH_3NH_3PbI_3$ perovskite film characterized by enlarged grains, minimized grain boundaries, low defect density, and uniform compactness. Concurrently, the hydrophobic properties of the perovskite film's interface are significantly enhanced. EA, with its high polarity and low boiling point, effectively promotes the rapid crystallization of perovskite and enhances the contact and stability among the functional layers of solar cells. On the other hand, the C=O functional group present in AA serves to passivate the coordinated Pb^{2+} defects and strengthen the interaction between cations and anions in the perovskite through coordinate bonds (see Fig. 3). This favorable interaction facilitates the formation of dense, large-grained films. Under the optimized concentration of AA (Fig. 4), the PCE of the fabricated $CH_3NH_3PbI_3$ PSCs increased from 19.2% to 21.1%, accompanied by improved stability in air.[39]

(d) In the perovskite treatment process, the integration of anti-solvent EA and additive isopropanol (IPA) notably enhances the surface morphology of the perovskite film. This treatment effectively passivates grain boundaries, ultimately

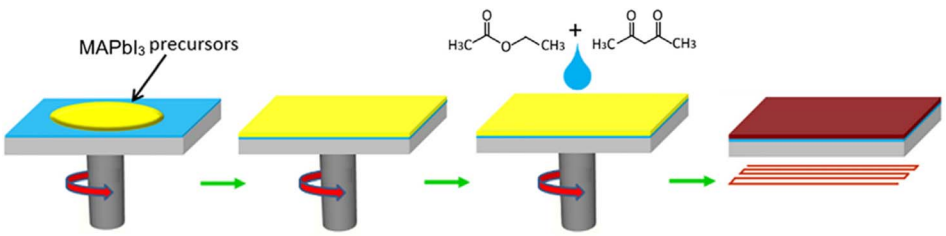

Fig. 3 Schematic diagram of the process of preparing perovskite thin films through EA + AA. The perovskite precursor solution is rotated onto a TiO_2/FTO substrate, and AA + EA is dropped onto the perovskite precursor thin film. After solvent quenching, it turns reddish brown. Annealing transforms into black perovskite phase. This figure has been reproduced from ref. 39 with permission from Elsevier, copyright 2022.

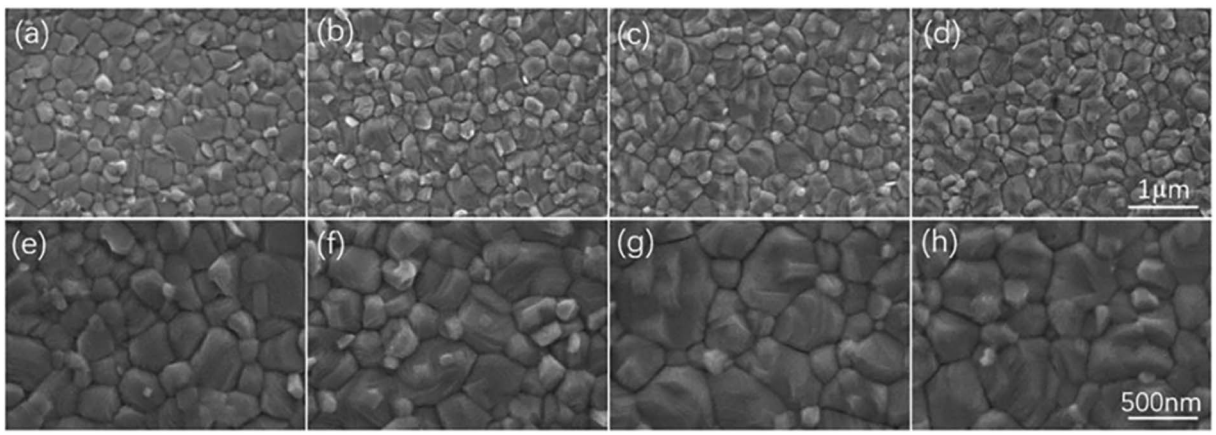

Fig. 4 Surface SEM images of $CH_3NH_3PbI_3$ thin films treated with different concentrations of AA at EA values of 0 (a and e), 0.5% (b and f), 1% (c and g), and 2% (d and h). This figure has been reproduced from ref. 39 with permission from Elsevier, copyright 2022.

yielding $CH_3NH_3PbI_3$ perovskite films characterized by exceptional crystallinity, enlarged grains, a smooth surface, and minimized grain boundaries. Among them, IPA exhibits weak polarity and a low boiling point, both of which contribute favorably to the rapid crystallization of perovskite. When using an optimized concentration of IPA, $CH_3NH_3PbI_3$ PSCs demonstrate exceptional performance, achieving a notable PCE of 18.98% under dry conditions. Notably, these devices exhibit negligible hysteresis and maintain excellent stability over a period of 30 days.[40]

(e) Treating perovskite with the anti-solvent EA, along with the addition of potassium thiocyanate (KSCN), results in increased grain size and crystallinity, fewer grain boundaries, and reduced trap states. Specifically, the KSCN additive slows down the growth process of perovskite, facilitating the formation of larger perovskite domains during the manufacturing process. These expanded domains, in turn, minimize the volume and surface trap density of the perovskite. It enables lower trap-assisted charge recombination and efficient charge extraction in solar cells. The volatile thiocyanate ions (SCN^-) arrange lead iodide (Pb–I) octahedrons due to the strong affinity between Pb^{2+} and SCN^-, thereby optimizing the morphology of the thin film. Furthermore, the K^+ alkali metal ions effectively passivate the grain boundaries and trap states of perovskite, thereby enhancing the stability and efficiency of solar cells. When utilizing an optimized concentration of KSCN, the fabricated $CH_3NH_3PbI_3$ PSCs exhibit a maximum PCE of 17.12%, along with improved stability in ambient air.[41]

3.1.2 $CH_3NH_3PbI_3$ perovskite films without ethyl acetate (EA). As research continues into the preparation of perovskite films using ASAC, scientists have discovered that numerous other organic solvents play a pivotal role in the production of these films. The resulting $CH_3NH_3PbI_3$ perovskite films boast impressive PCE.

(a) *Sec*-butyl ethanol (2-BA) is a colorless and transparent liquid with a scent similar to wine, boasting a boiling point of 99.5 °C and weak polarity. It is commonly used as a raw material for synthesizing perfumes and dyes, as well as an environmentally friendly solvent. By employing the anti-solvent 2-BA in the processing of perovskites, we have achieved high-quality perovskite films that exhibit no excess PbI_2, enlarged grain sizes, smoother surfaces, reduced trap-state densities, enhanced crystallinity, increased electron–hole recombination resistance, and superior charge carrier extraction capabilities. The PCE of the fabricated $CH_3NH_3PbI_3$ PSCs reached 19.29%, exhibiting exceptional moisture stability.[42]

(b) *N*-Propyl acetate (NPAC) belongs to the slightly toxic category with a high boiling point of 102 °C and a low saturated vapor pressure. PM is a low-toxicity ether with a high boiling point of 120 °C and no strong irritating odor (only a faint ether scent). Using green anti-solvents like Propylene glycol methyl ether (PM) or NPAC to treat perovskites effectively regulates their crystallization process, yielding calcium titanate films with large grain sizes, uniform density, and complete coverage. These anti-solvents enhance the nucleation of PbI_2 particles to varying degrees, offering heterogeneous nucleation sites for perovskite crystals and accelerating the nucleation process. As a result, the PCE of $CH_3NH_3PbI_3$ PSCs prepared with these anti-solvents reaches up to 21.60% and 20.05%, respectively, exhibiting superior photovoltaic performance and stability.[43]

3.2 Formamidine (FA) perovskite thin films with green anti-solvent

Firstly, the photoelectric properties of $FAPbI_3$ perovskite are truly exceptional. Formamidinium iodide, an organic compound, boasts excellent photoelectric performance and stability, whereas perovskite structural materials are inorganic substances renowned for their outstanding photoelectric capabilities. This unique combination positions $FAPbI_3$ perovskite as a standout performer in the realm of photoelectric conversion. Secondly, the crystal structure of $FAPbI_3$ perovskite is quite distinctive, comprising Pb, I, and FA, mimicking the classic ABO_3 perovskite arrangement. In this structure, the A-site is typically occupied by organic cations, like FA^+, while the B-site is held by $Pb2^+$. This unique configuration endows $FAPbI_3$ perovskite with a stable crystalline morphology and exceptional physical properties. Furthermore, $FAPbI_3$ boasts an optimal bandgap of 1.48 eV, with an absorption onset wavelength extending to a remarkable 840 nm. Its Goldschmidt tolerance factor hovering close to 1 signals robust structural stability and minimal distortion. Therefore, $FAPbI_3$ is widely considered as the leading perovskite composition with the potential to unlock record-breaking photocurrent densities and device efficiencies.[44–47]

(a) Methyl benzo-ate (MB) is a dual-function anti-solvent that boasts a high boiling point of 198 °C, low volatility, environmental friendliness, non-halogenated properties, and toxicity-free characteristics. Perovskite precursors, including MAI, FAI, and PbI_2, can be easily dissolved in pure MB, and their solubility can be further enhanced through heating. Hence, the anti-solvent MB serves dual purposes in the processing of perovskites. It acts as a rapid crystallization agent during the low-temperature spin-coating stage, facilitating the formation of crystal seeds. Additionally, it serves as a digestion solvent for dissolving perovskite precursors during the high-temperature annealing stage (see Fig. 5). This not only prevents the loss of organic components during thermal annealing but also effectively suppresses the formation of hybrid lead halide phases. This innovative dual-function anti-solvent is employed in planar n-i-p PSCs to create high-quality perovskite layers, enabling a remarkable power conversion efficiency of up to 22.37% while exhibiting negligible hysteresis and stability lasting over 1300 hours.[48]

(b) Methoxybenzene (PhOMe), a green solvent with a boiling point of 153 °C, stands out for its low toxicity, moderate saturated vapor pressure, and solvent properties akin to those of TL and *tert*-butylbenzene. As depicted in Fig. 6, perovskite films crafted using PhOMe as an anti-solvent exhibit smoother surfaces, larger grain sizes, and reduced carrier recombination rates compared to those treated with CB, all while maintaining consistent crystallinity and absorption characteristics. Consequently, the C_s/MA/FA PSCs fabricated with this method boast a PCE of 19.42%.[49]

(c) Isopropanol (IPA) exhibits characteristics such as weak polarity and a low boiling point, and it can induce rapid

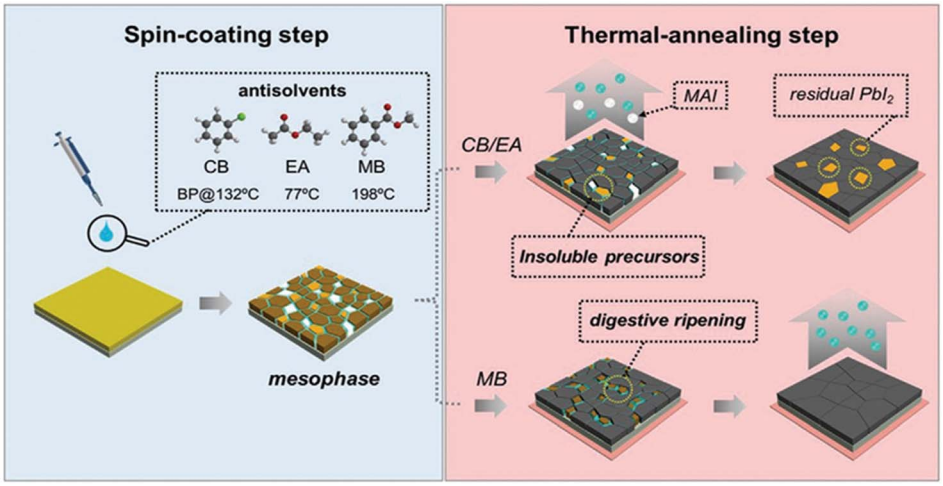

Fig. 5 Schematic comparison of CB, EA, MB anti-solvent treatment of perovskite films. Residual CB/EA may interrupt the solid solution secondary growth of perovskite crystals. Some organic components in the precursor of perovskite, such as MAI, tend to evaporate rather than form perovskite phase during annealing, leading to the transformation of perovskite into PbI_2. This figure has been reproduced from ref. 48 with permission from Wiley, copyright 2020.

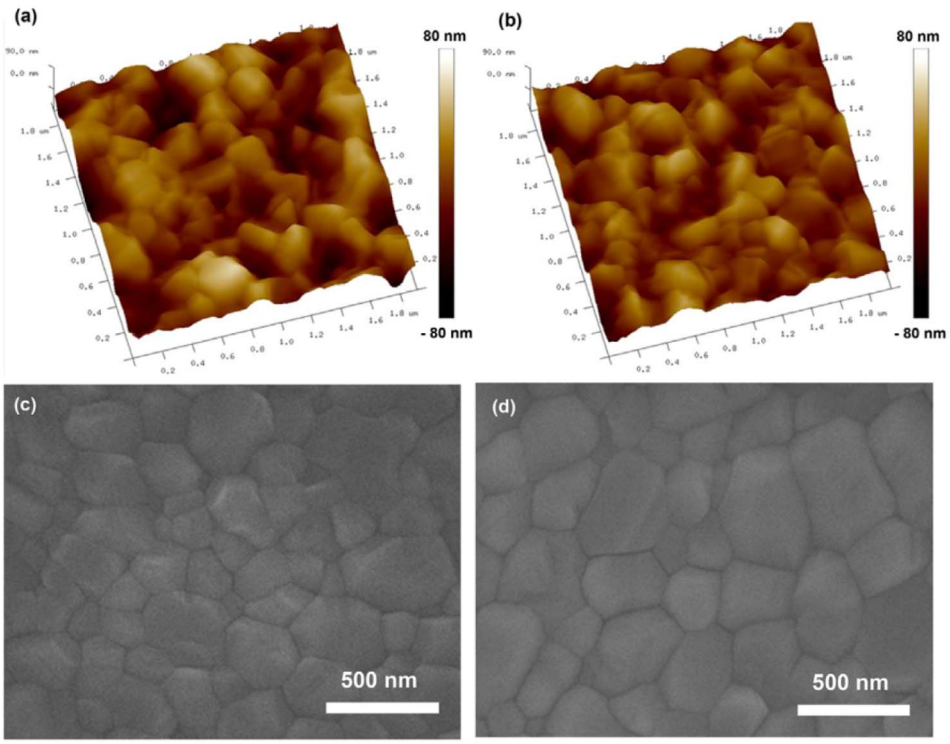

Fig. 6 Microstructure of perovskite thin films deposited on TiO_2/FTO substrates: AFM morphology images of (a) CB–P, (b) PhOMe–P, and corresponding surface SEM images of (c) CB–P, (d) PhOMe-P. This figure has been reproduced from ref. 49 with permission from Wiley, copyright 2018.

crystallization in perovskites. When used as a green anti-solvent IPA to treat $Cs_5(MA_{0.17}FA_{0.83})_{95}Pb(I_{0.83}\ Br_{0.17})_3$ perovskites, the resulting perovskite films exhibit a more uniform morphology with larger grain sizes. The fabricated $Cs_5(MA_{0.17}FA_{0.83})_{95}$-$Pb(I_{0.83}\ Br_{0.17})_3$ PSCs achieved a PCE of 21.50%, exhibiting exceptional moisture stability. Moreover, considering that PSCs consist of multiple layers processed with different solvents, researchers have also explored the feasibility of utilizing green solvents for the production of all layers of PSCs. The best PCE achieved with this fully green solvent processing method was 19.5%, establishing a new record for PSCs processed solely with green solvents.[50,51]

(d) Anisole (ANS), with a boiling point of 154 °C, exhibits low polarity. Researchers conducted an exhaustive comparison between anisole and the notoriously toxic yet frequently utilized CB and TL. The findings reveal that perovskite films crafted from anisole exhibit comparable performance to those utilizing CB and TL, achieving a stable PCE of 20.2%, marking the superior PCE attained when employing anisole. Furthermore, when processed under ambient conditions with ANS anti-solvent, the PSCs not only pose lesser toxicity risks but also maintain a robust PCE of up to 15.4%. This presented methodology offers a viable pathway towards establishing a reliable atmospheric deposition scheme for perovskites, all while mitigating potential health hazards associated with the system.[52]

(e) Acetic acid (HAc), with a boiling point of 117.9 °C, exhibits high polarity. When used as an anti-solvent in treating perovskites, HAc effectively controls the crystallization process, leading to the production of smoother, defect-free perovskite films with outstanding photoelectric performance. Not only does a small amount of HAc reduce the roughness of the perovskite film and residual PbI_2, but the electron-rich carbonyl group (C═O) in acetic acid also creates a passivation effect. The PCE of the fabricated $Cs_{0.05}FA_{0.80}MA_{0.15}Pb(I_{0.85}Br_{0.15})_3$ PSCs reached 22.0%, and the cells maintained 96% of their initial efficiency after being stored in an environment with controlled relative humidity (RH) of less than 30% for 2400 hours, without the need for any encapsulation.[53]

(f) Ethanol has a boiling point of 78.3 °C and a high polarity, and methylamine bromide (MABr) has a melting point between 248.0 °C and 253.0 °C. Treatment of perovskite with ethanol and MABr can improve the crystallinity of perovskite film grains, and the larger grain size can passivate its surface defects. The mixed anti-solvent of ethanol and MABr can modify $Cs_{0.15}FA_{0.85}PbI_3$ perovskite films, in which MABr can react with PbI_2 produced by perovskite and effectively inhibit the defect-induced non-radiation recombination. The PCE of $Cs_{0.15}FA_{0.85}PbI_3$ PSC is 21.53%, and the storage stability and light transmission stability are good.[54]

3.3 Perovskite thin films with tin (Sn)/antimony (Sb)/copper (Cu) instead of lead (Pb)

Due to the inherent toxicity of lead and the instability of Pb-based perovskites, their practical applications have been severely constrained by recent environmental regulations. Consequently, scientists have sought to experiment with alternative materials to replace lead, such as Sn, Sb and Cu. Due to the similarity in size and valence shell between divalent Sn cations and divalent Pb cations, Sn can be used as a substitute for Pb in the preparation of perovskite films. Additionally, trivalent Sb, with its similar electronic configuration to divalent Pb and its resistance to oxidation in atmospheric conditions, Sb-based perovskite derivative has already been developed as an indoor photovoltaic absorber, presenting opportunities for commercialization. So far, Cu has emerged as a promising candidate for replacing lead in Cu-based perovskite materials, given its low toxicity. The perovskites fabricated from these three materials have garnered significant research interest due to their low toxicity and exceptional photoelectric properties.

(a) The green anti-solvent diethyl carbonate (DEC) is a decarbonate of ethanol, a clear colorless liquid at room temperature with a boiling point of 126–128 °C and low polarity. The delayed kinetics of solvent-anti-solvent interactions enabled by the anti-solvent DEC slowed down the crystallization of $FASnI_3$ perovskite, leading to superior crystal orientation and reduced high-dimensional extension defects. More importantly, the special crystallization makes the distribution of Sn/I vacancies in perovskite films non-uniform, which leads to a gradient distribution of p-type self-doping on the upper surface but gradually from the upper surface to the lower surface. The resulting ribbon structure gradient facilitates carrier transport and suppresses the reverse charge accumulation between the two interfaces. The PCE of the prepared $FASnI_3$ PSCs reached 14.2% with good operational stability. And J_{sc} (short circuit current) = 24.2 mA cm^{-2}, V_{oc} (open circuit voltage) = 0.8 V, FF (filling coefficient) = 73.5%.[55]

(b) The crystallization process of Sn-based perovskites is carefully controlled through the utilization of the environmentally friendly anti-solvent, acetic acid (HAc). As depicted in Fig. 7, HAc serves a dual purpose. Firstly, it enhances the nucleation rate of the precursors by promoting salting-out crystallization. This occurs as hydrogen bonds form between HAc and the precursor solvent, weakening the solvation of SnI_2 by DMSO, and thereby increasing the effective concentration of pre-crystalline substances, leading to the precipitation of materials necessary for crystallization. Secondly, due to the slow volatilization of HAc during the annealing process, the hydrogen bonding between HAc and the organic ammonium salt delays the continued growth of the perovskite phase. Overall, this fast nucleation process and slow crystal growth process favors the preparation of high-quality Sn-based perovskite films. In addition, the unvolatilized residual HAc reduces the loss of organic amine salts and passivates the defective states in the perovskites. The boiling point of HAc is 117.9 °C, and the PCE of $FASnI_3$ PSC prepared with HAc reaches 12.78% (open-circuit voltage of 0.92 V in a non-chlorophenyl-based device).[56]

(c) Anti-solvent methoxybenzene (PhOMe) treatment $Cs_3Sb_2Cl_xI_{9-x}$ of perovskite can effectively increase the crystallization of perovskite films and regulate the crystallization process, and the surface morphology of the prepared films is dense, with better light absorption properties. Its devices can achieve a PCE of 2.07% for $Cs_3Sb_2Cl_xI_{9-x}$ PSCs prepared with low-cost carbon electrodes, which is an improvement of 470% compared to 0.44% for a control device without anti-solvents, and also exhibits good thermal and air stability without humidity control.[57]

(d) Treatment of $Cs_3Cu_2I_5$ perovskites with the green anti-solvent methyl acetate (MA) and dropping MA at the end of the spin-coating process yielded perovskite films with small surface roughness and uniform smoothness, as shown in Fig. 8. Among them, MA has the properties of low toxicity, low boiling point (56.9 °C) and high vapor pressure (28.8 kPa), which can increase the vapor pressure, lower the boiling point of the

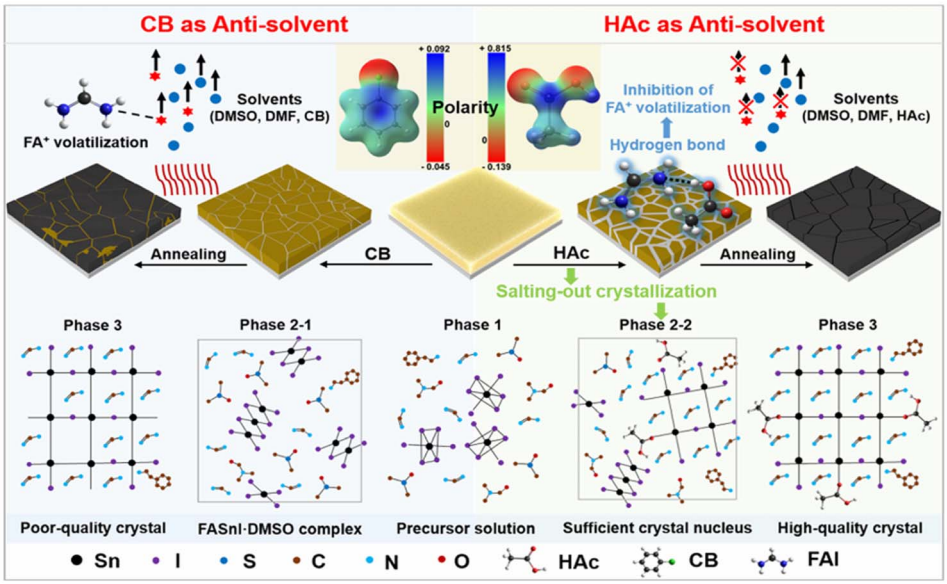

Fig. 7 The procedure scheme of preparing perovskite films with CB or HAc as an anti-solvent and the composition of the film before and after each step. Phase 1: the thin film consists of colloidal precursors of photoinactive solid precursors (SnI_2, FA^+ and PEA^+) and liquid solvents DMSO and DMF. Phase 2–1: the thin film consists of a solvent-complex, liquid solvents and anti-solvent (CB). Phase 2–2: the thin film consists of a perovskite crystal nucleus, solvent-complex, liquid solvents and anti-solvent (HAc). Phase 3: crystallized perovskite film. This figure has been reproduced from ref. 56 with permission from Royal Society of Chemistry, copyright 2023.

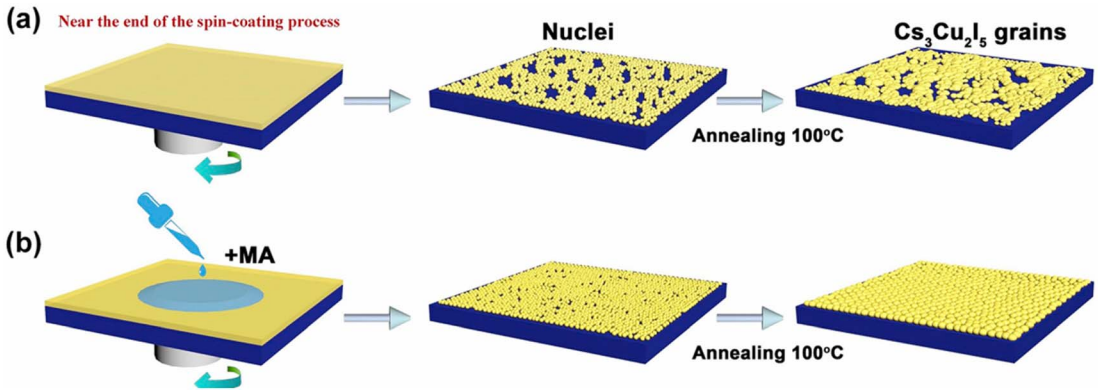

Fig. 8 Growth and grain growth of $Cs_3Cu_2I_5$ perovskite film with/without MA, (a) without MA. (b) With MA. This figure has been reproduced from ref. 58 with permission from Elsevier, copyright 2020.

solution, accelerate the crystallization of $Cs_3Cu_2I_5$ perovskite, and prepare $Cs_3Cu_2I_5$ perovskite thin films with uniform morphology. The prepared $Cs_3Cu_2I_5$ PSCs achieved a PCE of 15.1% and exhibited long-term air stability.[58,59]

Among the entire spectrum of anti-solvents discussed, the key to achieving higher PCE in PSCs using green anti-solvents lies in selecting the right ones and optimizing their application procedure. When it comes to selecting green anti-solvents, it's essential to have a deep understanding of the interplay between the anti-solvent and the perovskite precursor material. Recognizing that the relative solubility of precursor components within different anti-solvents is crucial to film formation, when the solubility of anti-solvent and organic precursor is high, a large amount of organic halides are also removed by these anti-solvents with the precursor solution, which destroys the microstructure of the film and leaves PbI_2 that cannot be converted into perovskite. Furthermore, we can fine-tune this effect by adjusting the duration of the anti-solvent application rate. Due to the irreversible change in chemical metering, a faster dripping rate of the anti-solvent leads to higher efficiency. Conversely, in cases where the solubility with the organic precursor is low, a slower dripping rate of the anti-solvent results in better extraction of the precursor solution. If the dripping rate is too fast, it can lead to more residue of the precursor solution.

Based on this principle, researchers observed that when using a single anti-solvent, there would still be a large number of grain boundaries formed. During the thermal annealing

Table 2 Properties of perovskite films prepared with green anti-solvents and related process parameters [R_q (root mean square roughness), J_{sc} (short circuit current), V_{oc} (open circuit voltage), FF (filling coefficient), PLQY (photoluminescence quantum efficiency)]

Perovskite type	Type of anti-solvent	Morphological characteristics	Dosage and service time of anti-solvent	Research highlights	Performance parameter	Stability	Ref.
$CH_3NH_3PBI_3$	*Sec*-butyl ethanol (2-BA, used in N_2-filled glovebox)	Larger grain size, smooth surface (R_q = 8.9 nm)	In the second spin coating, add 250 μL of 2-BA	Eliminate residual and reduced PbI_2	PCE = 19.29% J_{sc} = 22.84 mA cm^{-2} V_{oc} = 1.12 V FF = 75.40%	75% of initial PCE (without packaging, 10 days)	42
$CH_3NH_3PBI_3$	Propylene glycol methyl ether (PM, used in N_2-filled glovebox)	Uniform and dense grain size, complete coverage, low surface roughness	After spin coating, 150 μL was dripped	Promote the nucleation of PbI_2	PCE = 21.60% J_{sc} = 25.80 mA cm^{-2} V_{oc} = 1.12 V FF = 75%	None	43
$CH_3NH_3PBI_3$	*N*-Propyl acetate (NPAC, used in N_2-filled glovebox)	Uniform and dense grain size, complete coverage, low surface roughness	After spin coating, 150 μL was dripped	Provide heterogeneous nucleation sites	PCE = 20.05% J_{sc} = 25.10 mA cm^{-2} V_{oc} = 1.12V FF = 72%	None	43
$CH_3NH_3PBI_3$	Ethyl acetate (EA, used in air)	Low density trap state, dense, relatively smooth (R_q = 8.76 nm)	After spin coating, 300 μL was dripped	One of the best PCE of completely ambient-processed ZnO-planar device	PCE = 17.75% J_{sc} = 22.20 mA cm^{-2} V_{oc} = 1.082 V FF = 74%	90% of initial performance (air storage, 50 days)	36
$CH_3NH_3PBI_3$	Ethyl acetate (EA, used in air and glovebox)	Faster charge separation, improved electron transport	After spinning for 10 seconds, add 60 μL dropwise, then add 150–200 μL dropwise	Good voltage responsiveness under 0.05% sunlight	PCE = 18.46% J_{sc} = 22.49 mA cm^{-2} V_{oc} = 1.10 V FF = 75%	85% of initial performance (air storage, 50 days)	38
$CH_3NH_3PBI_3$	EA + acetylacetone (AA, used in N_2-filled glovebox)	Dense thin film	In the second spin coating step, add 0.3 mL EA/AA dropwise	Passivation defect	PCE = 21.10% J_{sc} = 24.48 mA cm^{-2} V_{oc} = 1.120 V FF = 76.95%	87% of initial PCE (without packaging, 1224 hours)	39
$CH_3NH_3PBI_3$	EA + IPA (used in N_2-filled glovebox)	Large grain size, smooth, compact morphology (R_q = 10.2 nm)	After rotation, add 0.1 mL dropwise	Improve photoelectric performance	PCE = 18.98% J_{sc} = 22.00 mA cm^{-2} V_{oc} = 1.08V FF = 79.9%	90% of initial PCE (without packaging, 30 days)	40
$CH_3NH_3PBI_3$	EA + potassium thiocyanate (KSCN, used in N_2-filled glovebox)	Low surface defect density, fewer grain boundaries	Add 120 μL dropwise onto the perovskite layer	Delaying the growth of perovskite	PCE = 17.12% J_{sc} = 19.73 mA cm^{-2} V_{oc} = 1.143 V FF = 75.90%	90% of initial PCE (after 1080 hours, 20–30% RH)	41
$(FA_{0.85}MA_{0.15})PB(I_{0.85}BR_{0.15})_3$	Methyl benzoate (MB, used in N_2-filled glovebox)	Uniform nucleation, large grain size	In the first spin coating, drip in 100 μL	Nontoxic bifunctional anti-solvent	PCE = 22.37% J_{sc} = 24.46 mA cm^{-2} V_{oc} = 1.22 V FF = 74.95%	94% of initial PCE (50 ± 10% RH and 25 ± 5 °C, 1350 hours)	48
$Cs_{0.05}(MA_{0.17}FA_{0.83})_{0.95}Pb(I_{0.83}Br_{0.17})_3$	Isopropanol (IPA, used in N_2-filled glovebox)	Uniform, pinhole free surface morphology, smooth top surface of the film, large grain size	In the second spin coating, add 100 μL dropwise	Pure green solvent	PCE = 21.50% J_{sc} = 23.69 mA cm^{-2} V_{oc} = 1.11V FF = 82.14%	None	50 and 51

Table 2 (*Contd.*)

Perovskite type	Type of anti-solvent	Morphological characteristics	Dosage and service time of anti-solvent	Research highlights	Performance parameter	Stability	Ref.
$Cs_{0.05}(MA_{0.17}FA_{0.83})_{0.95}Pb(I_{0.83}Br_{0.17})_3$	Anisole (ANS, used in argon-filled glovebox)	Uniform and smooth film	Add 200 μL dropwise during the last 10 seconds of spin coating	Proving a completely non halogenated solvent system, ANS serves as both an anti-solvent and a solvent	PCE = 19.42% J_{sc} = 23.5 mA cm^{-2} V_{oc} = 1.14 V FF = 76%	92% of initial PCE (stored in glove box within 112 h)	52
C_s/MA/FA	Methoxybenzene (PhOMe, used in N_2-filled glovebox)	Good uniformity and large grain size (R_q = 16.3 nm)	Drip before the spin coating program ends	Low toxicity and good efficacy	PCE = 19.42% J_{sc} = 22.78 mA cm^{-2} V_{oc} = 1.10 V FF = 77.52%	None	49
$Cs_{0.05}FA_{0.80}MA_{0.15}Pb(I_{0.85}Br_{0.15})_3$	Acetic acid (HAc, used in N_2-filled glovebox)	Ultra-uniform surface, little PbI_2 deposition	During the spin coating process, add a mixed solution of 8 v% Ac dropwise	Multi-functional solvent crystallization	PCE = 22% J_{sc} = 23.2 mA cm^{-2} V_{oc} = 1.19 V FF = 79.6%	96% of initial PCE (after 2400 hours of storage in RH <30%)	53
$CS_{0.15}FA_{0.85}PBI_3$	Ethanol + methylamine bromide (MABr–Eth, used in Ar atmosphere)	Large grain size, high crystallinity, significant differences in different grain shapes	Add 80 μL dropwise during the last 10 seconds of spin coating	Eliminate residual PbI_2	PCE = 21.53% J_{sc} = 25.07 mA cm^{-2} V_{oc} = 1.09 V FF = 78.79%	80% of initial PCE (stored in glove box within 20 days)	54
$FASNI_3$	Diethyl carbonate (DEC, used in N_2-filled glovebox)	P-Type self doping gradient distribution	Spin coating	Solvent anti-solvent delay kinetics	PCE = 14.2% J_{sc} = 24.2 mA cm^{-2} V_{oc} = 0.8 V FF = 73.5%	95% of initial efficiency after 200 hours of air lighting	55
$FASNI_3$	Acetic acid (HAc, used in air)	Low defect density	Add 150 μL to the precursor solution	Salt precipitation crystallization accelerates solution nucleation	PCE = 12.78% J_{sc} = 18.84 mA cm^{-2} V_{oc} = 0.92 V FF = 73.72%	90% of initial PCE (N_2 glove box, 4000 hours)	56
$CS_3SB_2CL_XI_{9-X}$	Methoxybenzene (PhOMe, used in N_2-filled glovebox)	Dense surface, good crystallinity	After spin coating for about 8 seconds, dispense 65 μL PhOMe to the lower layer	Low-cost carbon electrode with excellent performance	PCE = 2.07% J_{sc} = 4.47 mA cm^{-2} V_{oc} = 0.84 V FF = 55.20%	75% of the initial PCE (240 h at room temperature)	57
$CS_3CU_2I_5$	Methyl acetate (MA, used in N_2-filled glovebox)	Small surface roughness, small and uniform grain size range, no pores	After the second rotation, add 100 μL	Excellent low toxicity performance	PCE = 15.1% PLQY = 76.0%	88.6% initial PLQY (after two months of storage)	58 and 59

stage, the residual anti-solvent in the perovskite film would have an adverse effect on the growth of perovskite crystals, resulting in poor crystallinity. Additionally, organic constituents in the perovskite precursor, such as methylammonium iodide (MAI), are prone to volatilization during annealing, leading to the formation of PbI_2 rather than the perovskite phase. This phenomenon indicates the presence of certain Pb^{2+} defects, and contributes to poor film quality and hydrophobicity.

To tackle these challenges, researchers have experimented with additives. The addition of additives can effectively passivate the uncoordinated Pb^{2+} defects and strengthen the ionic interactions within the perovskite structure, significantly improving the surface morphology of the perovskite film and thereby facilitating the formation of dense large-grain films. Currently, most of such research achievements focus on $CH_3NH_3PbI_3$ PSCs, while there are still limited reports on FA-based PSCs and perovskite materials doped with Cu, Sn, *etc.*, which require further research by relevant personnel (Table 2).

4 Green preparation of perovskite films without anti-solvent

Although the above methods have indeed promoted the production of perovskite films, the need for precise control over the timing, speed, and volume of the anti-solvent dripping often leads to an increase in surface defects within the perovskite films, subsequently compromising the PCE and stability of the battery. To address this challenge, the green non-anti-solvent method for fabricating perovskite films has achieved extensive attention.[60–64] By optimizing the manufacturing process, these physical techniques enable the production of high-quality films without anti-solvents or additional harmful substances, minimizing surface defects and boosting the photovoltaic performance of the cells.[65–70]

In fabricating perovskite films *via* the green non-anti-solvent method, the crucial aspect lies in the precise regulation of the film's structure, grain size, and crystallinity.[71–73] Presently, the most commonly adopted methods include two-step method, gas-assisted techniques, high-temperature annealing, confined-space annealing strategy, and seed-assisted. Each of these methods boasts unique characteristics, and with their comprehensive utilization and ongoing refinement, they are anticipated to furnish more reliable and efficient solutions for the production of PSCs.

4.1 Gas-assisted

A simple gas-assisted solution processing technique can effectively address these challenges. This method facilitates rapid solvent evaporation and promotes rapid supersaturation precipitation, altering the nucleation and crystal growth dynamics of perovskite during the spin-coating process. Ultimately, it yields highly uniform perovskite films composed of densely packed single-crystal grains. Cheng *et al.* conducted research on the preparation of $CH_3NH_3PbI_3$ films using a gas-assisted method without the use of an anti-solvent, resulting in perovskite films with excellent substrate coverage and achieving a PCE of 17.0% for their PSCs.[74,75] Furthermore, researchers have explored the utilization of hot airflow during the perovskite nucleation phase to fabricate pinhole-free $CH_3NH_3PbI_3$ perovskite layers. By employing hot air, they are able to stimulate the growth of uniformly distributed nuclei, ultimately leading to the production of pinhole-free planar perovskite layers. Park[76] *et al.* incorporated a heated airflow into the spin-coating process of a MAI:$PbCl_2$ precursor solution, successfully fabricating pinhole-free mixed-halide $CH_3NH_3PbI_{3-x}Cl_x$ perovskite films through a one-step method. The PCE of their PSCs reached 19%.[77] Peter Amalathas *et al.* conducted research on the preparation of $CH_3NH_3PbI_3$ films using vapor-phase deposition without the use of an anti-solvent. They modified the perovskite film deposition process by inducing the formation of an intermediate $CH_3NH_3PbI_3 \cdot MACl \cdot xCH_3NH_2$ liquid phase through the combined use of CH_3NH_2 gas treatment and MACl additives. By adjusting the incorporation of MACl additives in the perovskite precursor solution, this intermediate liquid phase is able to effectively control the growth of 3 μm large grains in the $CH_3NH_3PbI_3$ perovskite films, resulting in a highly uniform morphology and increased crystallinity.[78] The PCE of PSCs prepared by this method can reach 21.0%.[79–81]

4.2 High temperature annealing

Annealing serves as a crucial step in the preparation of perovskite thin films, where temperature control has a direct impact on the film's crystallinity, morphology, optoelectronic performance, and long-term stability. The precise regulation of annealing temperature is paramount in optimizing film quality, elevating the performance of optoelectronic devices, and advancing the application of perovskite materials. Scientists have conducted thorough research on the structural evolution, phase transitions, and alterations in optoelectronic properties of perovskite films under various annealing temperature conditions, leveraging systematic experimental designs and refined analytical methods.

Eperon *et al.* investigated the relationship between annealing temperature within the range of 90 to 170 °C and the coverage rate of perovskite.[82] Dualeh *et al.* explored the influence of annealing temperatures ranging from 60 to 200 °C on the morphology of thin films, while Xu[83] *et al.* reported that a low-temperature gradual annealing method is highly effective in producing high-performance PSCs. Exposure to high temperature for long time, perovskite films tend to decompose into PbI_2 or residues. However, transient high temperature is conducive to the rapid volatilization of solvents and overcome the potential barrier of crystal phase formation.[84] Kim *et al.* introduced a simple process based on high-temperature short-time annealing (HTSA) for fabricating high-performing PSCs (see Fig. 9). Compared to perovskite films produced through low-temperature annealing, it provides a denser, brighter, and larger domain size perovskite film. The PCE of its PSCs reaches 18%.[85] Moreover, the HTSA process enables the deposition of uniform perovskite films over a wide range, providing a potential for the scaled-up production of PSCs. In this direction, Troughton *et al.* proposed a method to crystallize perovskite films through short-time exposure to high-intensity near-

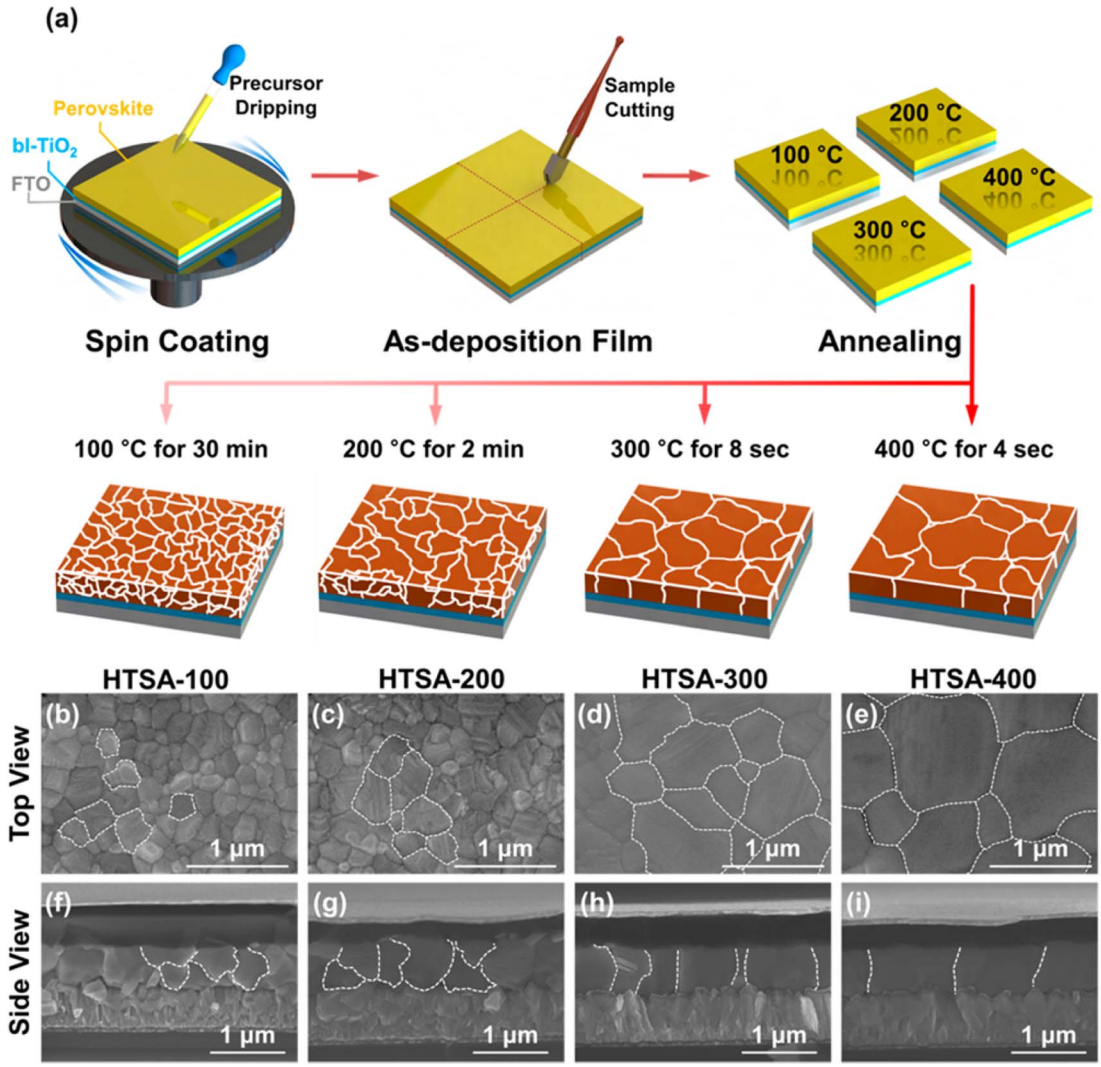

Fig. 9 (a) Schematic illustration of the annealing processes. (b–e) Surface SEM images (top view) of the perovskite films fabricated through HTSA-100, HTSA-200, HTSA-300, and HTSA-400 and (f–i) their cross-sectional images (side view), respectively. This figure has been reproduced from ref. 85 with permission from American Chemical Society, copyright 2017.

infrared radiation.[86] Abate *et al.* employed infrared annealing (FIRA) to synthesize $CH_3NH_3PbI_3$ perovskite films.[87] The PCE of PSCs fabricated through such methods can reach 24%.[88,89]

4.3 Confined-space annealing strategy (CSA)

In the CSA process, the reaction process on the sample glass sheet can be limited to a closed space, this allows for the controlled evaporation rate and direction of the internal solvent, ultimately leading to the production of high-quality perovskite films.

Wang *et al.* employed a universal CSA strategy applicable to various bandgaps of perovskites to fabricate high-quality perovskite absorbers, featuring enlarged grain size, improved crystallinity, and extended carrier lifetime (see Fig. 10b–d). The principle involves orienting the surface of the intermediate-phase perovskite film towards a solvent-permeable cover during the annealing process. Through a gradual solvent release process, a high-quality perovskite absorber layer is obtained, enabling the production of efficient single-junction PSCs (PVSCs) and all-perovskite tandem solar cells. High-performance, low E_g mixed Sn–Pb, and translucent wide E_g PSCs have been achieved, with PCE of 4-terminal (4-T) and 2-terminal (2-T) all-perovskite tandem solar cells reaching up to 25.15% and 25.05% respectively.[90] Deli *et al.* provided a feasible and convenient method for controlling the nucleation and growth process of perovskite grains by introducing the annealing process of perovskite films assisted by conductive glass. This novel annealing method does not involve any additives or the insertion of special substrates. The optimized device efficiency reached 15.77%.[91] Due to the hydrophilicity of perovskite materials, environmental humidity is an inevitable issue in the production process of PSCs. Gao *et al.* deliberately designed a novel CSA strategy that confines the space to control the amount and direction of MACl as shown in the Fig. 10a, maintaining evaporation rate at a low level. This method

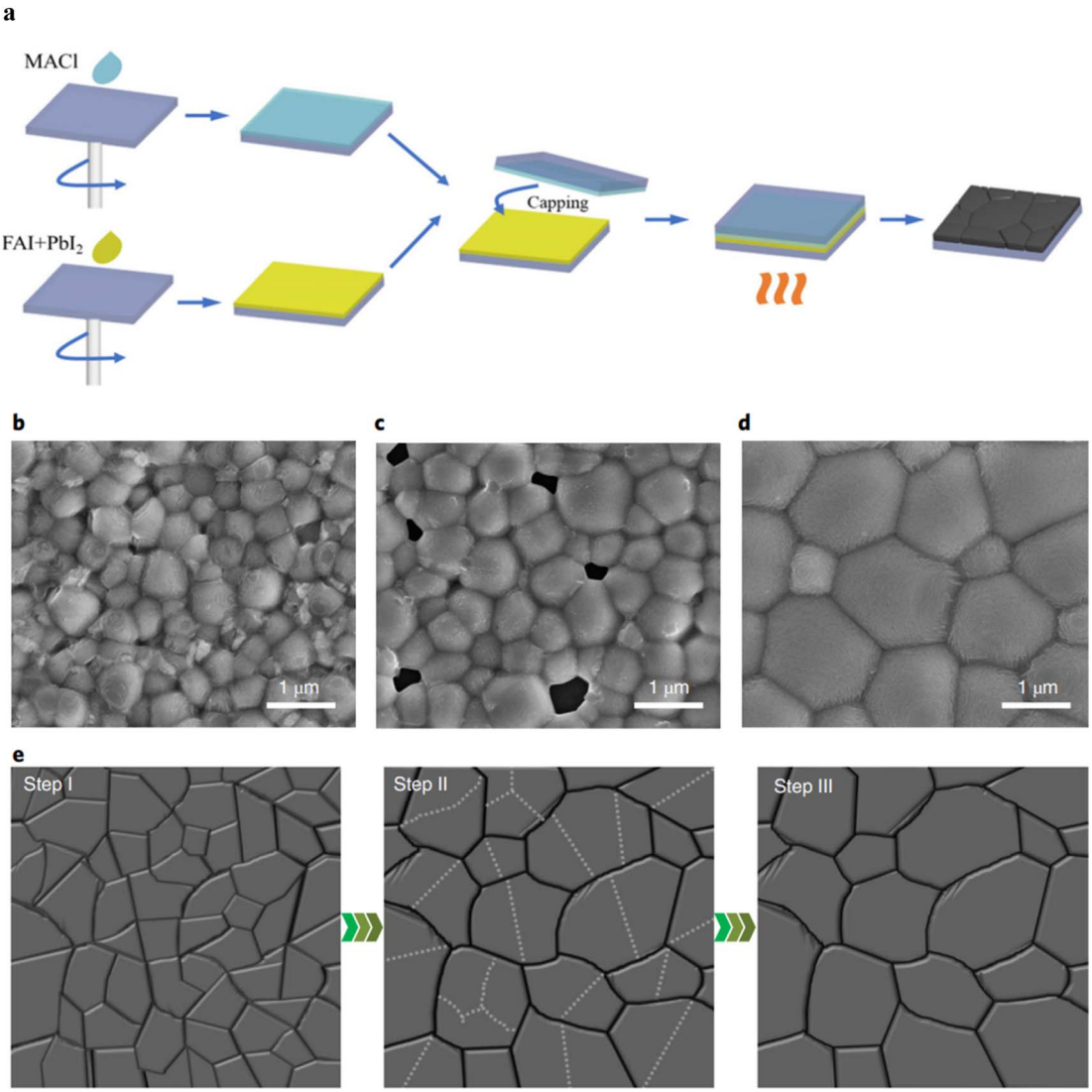

Fig. 10 (a) Schematic of experimental procedures for MACl-CSA films. Scheme of normal annealing, solvent annealing and CSA processes. (b–d) Top view SEM images of mixed Sn–Pb perovskite films fabricated with normal annealing (b), solvent annealing (c) and CSA (d) processes. The scale bar is 1 μm. (e) Mechanisms of grain growth during the CSA process. This figure has been reproduced from ref. 90 and 91 with permission from Nature Publishing Group and Royal Society of Chemistry, copyright 2022 and 2024.

eliminates accidental pinholes caused by MACl evaporation, resulting in a dense $FAPbI_3$ film with excellent crystallinity and stability, free of the δ-phase. Finally, a perovskite solar cell with a PCE of 17.27% was achieved in humid air.[92]

4.4 Seed-assisted

The seed-assisted strategy can lower the formation energy of perovskite crystallization, making that perovskite films is more prone to promoted preferential growth of crystal planes, suppressed impurities and improved crystallinity, providing a strong guarantee for the high-quality perovskite films.

Liu *et al.* introduced an innovative self-disintegrating seed method, utilizing 4-fluorobenzylammonium iodide (4-FBZAI) to synthesize 2D RP perovskite $(4\text{-FBZA})_2PbI_4$, and then incorporated $(4\text{-FBZA})_2PbI_4$ as a seed into the PbI_2 film. During the process of perovskite crystal growth, $(4\text{-FBZA})_2PbI_4$ decomposes, releasing 4-FBZA^+ ions that effectively eliminate residual 2D perovskite from the 3D perovskite film. The liberated 4-FBZA^+ migrates to the perovskite interface, anchors onto the perovskite lattice, relieving lattice stress, passivating interfacial defects, and enhancing hole migration. With the synergistic action of the self-disintegrating seeds, the optimized device achieves a PCE of 23.73%.[93]

The research conducted by Siraj *et al.* introduces a novel method to achieve a highly stable black phase of $FAPbI_3$, even at temperatures significantly below the transition point from δ-$FAPbI_3$ to α-$FAPbI_3$. This method involves templating the Pb–Pb atomic spacing of 3D $FAPbI_3$ to closely match the Pb–Pb spacing of a carefully selected FA-based 2D perovskite. They broadened this templating strategy to scalable solution-processing techniques by incorporating prefabricated 2D perovskite seeds into the $FAPbI_3$ precursor solution. During the film formation, the phase-stable 2D perovskite initializes nucleation first due to its reduced formation

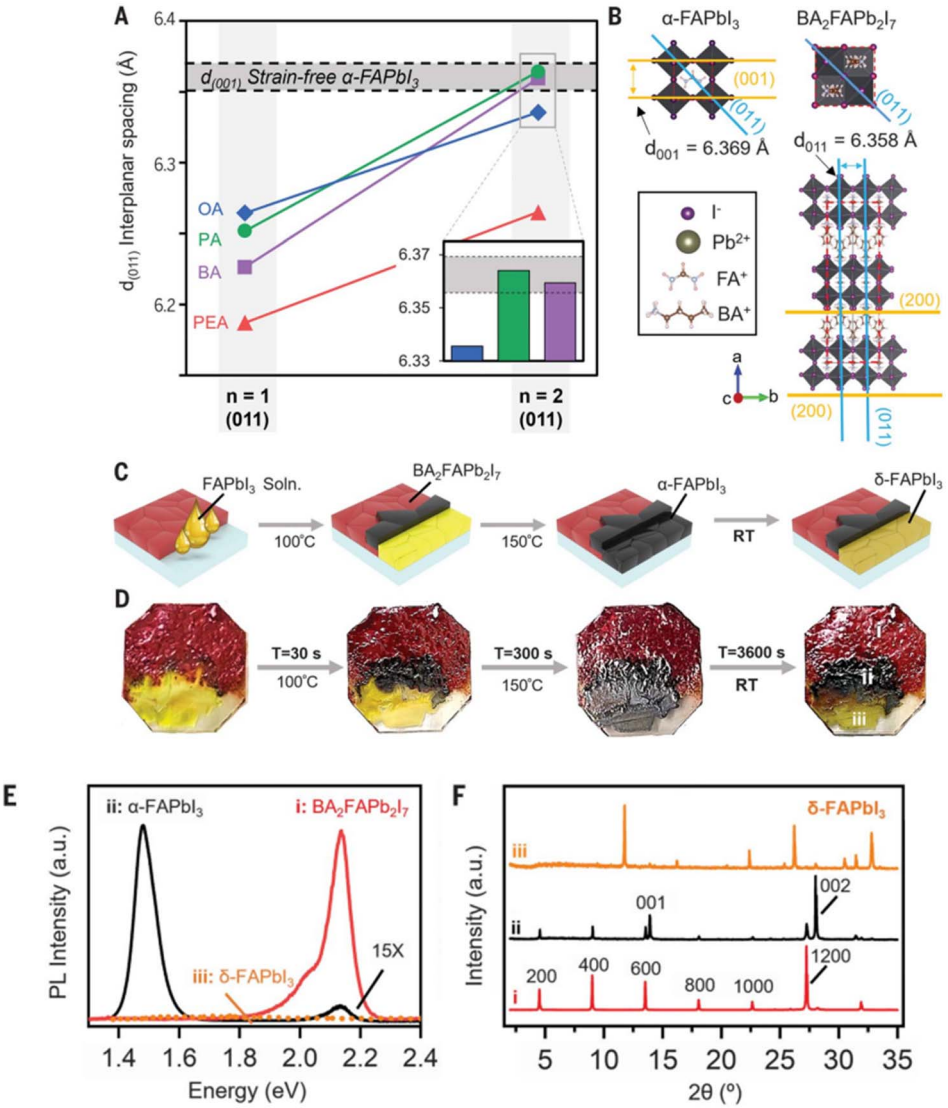

Fig. 11 Design principle and proof of concept for 2D perovskite lattice templating of $FAPbI_3$. (A) The $d_{(011)}$ interplanar spacing for $n = 1$ and FA-based $n = 2$ 2D perovskites with various A′ cations: PA, BA, OA, and PEA. (B) Diagram of the unit cells of $FAPbI_3$ (left) and $BA_2FAPb_2I_7$ (right). (C) Schematics of the templated $FAPbI_3$ drop-coating experiment. (D) Corresponding photographs of the experiment in (C) showing the three distinct regions of the substrate: region i, $BA_2FAPb_2I_7$ without $FAPbI_3$ solution; region ii, $BA_2FAPb_2I_7$ below $FAPbI_3$ solution; and region iii, $FAPbI_3$ solution on bare glass. (E) PL and (F) XRD of regions i–iii after 1 hour of exposure to ambient air, showing that the α-$FAPbI_3$ was stabilized when deposited on top of $BA_2FAPb_2I_7$. a.u., arbitrary units. This figure has been reproduced from ref. 94 with permission from American Association for the Advancement of Science, copyright 2024.

enthalpy and stability at ambient temperatures. Serving as a seed, the 2D structure allows the 3D perovskite to adopt the underlying 2D lattice periodicity, facilitating preferential templating of the 3D perovskite onto the 2D phase during subsequent film annealing. The resulting $FAPbI_3$ film achieved a PCE value of 24.1% in a p-i-n device structure with a device area of 0.5 cm^2 (Fig. 11).[94]

Yan *et al.* introduced a novel heterogeneous seed-assisted $FAPbI_3$ crystallization strategy, induced by DAP additives, for fabricating highly efficient inverted PSCs. In this method, the robust interaction between 2,4-diaminopyrimidine (DAP) and perovskite inhibits the formation of solvent-dominated intermediate phases, thereby favoring the creation of DAP–FA^+ $[PbI_3]^-$ (δ) heterogeneous seeds. These seeds swiftly transition to the desired α-phase during the initial formation stage, greatly aiding the subsequent crystallization process. Consequently, we achieve a highly crystalline α-$FAPbI_3$ film that boasts reduced trap density, extended carrier lifetime, and an impressive PCE of up to 25.29%. Additionally, this method significantly enhances the stability of the inverted device.[95]

4.5 Two-step method

In the exploration of green perovskite film fabrication techniques sans antisolvents, the two-step method stands out as a highly efficient and adaptable strategy, revealing tremendous

potential. It not only sidesteps the quality control hurdles posed by rapid solvent evaporation and phase separation in conventional methods but also enables precise tuning of film morphology, structure, and performance through a series of well-defined steps. The strong nucleation control offered by the two-step approach allows for independent manipulation of each stage, thereby bolstering the controllability of the nucleation process. By incorporating MAI (or alternative organic cation halides) and facilitating their reaction with PbI_2 to yield the perovskite phase, the nucleation process can be carried out under milder and more controllable conditions, which helps to reduce defects and impurities during the nucleation process.

Burschka *et al.*[96] first used two-step method to deposit lower TiO_2 layer on transparent conductive oxide coated glass substrate through aerosol spray pyrolysis technology, and obtained a device with PCE of 15%. In the first step of the two-step method, the crux lies in the formation of a uniform and dense PbI_2 precursor film on the substrate *via* solution spin-coating, spray coating, or other deposition techniques. In the second step, without the need for an anti-solvent, MAI (or other organic cation halides) are introduced into the deposited PbI_2 film *via* methods such as solution immersion, or secondary spin-coating, and immersed subsequently into an MAI solution, allowing for *in situ* formation of $CH_3NH_3PbI_3$. Furthermore, the morphology, crystallinity, and optoelectronic characteristics of the perovskite film can be further tailored through the incorporation of suitable additives or modifications to the solvent system. Yan *et al.*[97] utilized guanidinium benzoate (GBA) as an additive in a two-step approach, where GBA effectively blocks the hydration pathway of perovskite at the source, enabling the full realization of highly efficient PSCs in ambient conditions. GBA notably eliminates perovskite vacancies, boosts the binding energy between perovskite and H_2O, and mitigates the adverse impact of moisture on perovskite crystallization, ultimately yielding devices with a remarkable PCE of 25.32%.

The two-step method necessitates meticulous control over the evaporation rates of organic and inorganic precursors to achieve the appropriate stoichiometry in the deposited film. The gas-phase assisted method can more accurately control the content of components and the thickness of the film, avoiding the use of toxic solvents. It can also quickly prepare high-quality perovskite films at lower temperatures, reducing environmental pollution during the preparation process. Hu *et al.*[98] demonstrated a simple sequential vapor deposition (SVD) method for growing high-quality $CH_3NH_3PbI_3$ thin films, enabling all-vapor, low-temperature fabrication of planar PSCs without hole conductors. The nanoporous nature of the vapor-deposited PbI_2 film possesses a large specific surface area, allowing for easy penetration and contact with MAI vapor, thereby facilitating rapid and more uniform reactions between PbI_2 and MAI. This results in a phase-pure $CH_3NH_3PbI_3$ film that is pinhole-free, uniform, and smooth. Pérez-Gutiérrez *et al.* placed the lead halide film deposited by spin coating face-to-face with the methylamine halide film separated by a few millimeters. The system was placed under vacuum and heated to sublime the methylamine halide onto the lead halide film. This method allows for the deposition of uniform and dense perovskite films. It also simplifies the deposition of perovskite films and halide mixtures by using only two precursor materials. In addition, the sublimation time determines the substitution and final ratio between halides. By selecting the appropriate sublimation time, solar cells and LED devices can be prepared.[99] Liu *et al.* conducted a systematic study examining the effects of vapor pressure, various organic salt compositions, reaction time, and post-deposition processes on the quality of perovskite films and device performance. This resulted in the successful realization of CVD-based perovskite photovoltaic devices with an inverted structure, achieving an impressive PCE of up to 18.1%.[100]

5 Conclusion and prospect

Given the demands of sustainable development, the utilization prospects exhibited by PSCs are indeed impressive. High crystallinity, low defect density, and large grain sizes in perovskite films are crucial prerequisites for achieving high-performance solar cells. Among the various techniques available, the ASAC method stands out as one of the most widely utilized methods for obtaining high-quality perovskite films. In this article, we initially introduce the preparation of perovskite films, focusing on the use of $CH_3NH_3PbI_3$ as the perovskite material. Alternatively, we explore modifying the organic solvent in FA-based perovskite materials. Throughout the process, multiple green anti-solvents are employed, and both the preparation of films without additives and with various additives are examined. Subsequently, the article delves into the utilization of green anti-solvents for the fabrication of perovskite films, in which Sn and other elements are employed to replace the conventionally used Pb substrates. Notably, the batteries produced from these films boast impressive PCE. At the same time, the effect of preparing PSCs without anti-solvent is also very significant.

Pushed forward by technological innovation, the relentless progress in materials science, chemical engineering, and nanotechnology is anticipated to spawn the creation of even more novel green anti-solvents. These anti-solvents will exhibit superior environmental stability, heightened solubility capabilities, and reduced toxicity levels. Additionally, the exploration of perovskite materials themselves will continue to deepen, harnessing strategies like element doping and interface engineering to further elevate the photoelectric performance and stability of perovskite films. Collectively, these technological advancements will propel the performance of PSCs to unprecedented heights. Concurrently, optimizing the manufacturing process is crucial for achieving large-scale production and commercialization of PSCs. This entails enhancing the automation level of the production process, reducing production costs, improving production efficiency, and ensuring product consistency. To address the sensitivity of green anti-solvents to oxygen and water, more advanced encapsulation technologies and storage methods can be developed to ensure that PSCs maintain stable performance over extended periods. As we push forward the development of PSC technology, it's absolutely crucial to fully consider its environmental friendliness and sustainability. This includes adopting even more eco-friendly raw materials, minimizing harmful emissions during the

production process, and maximizing resource utilization efficiency. Additionally, we need to pay close attention to the recycling and disposal of PSCs after they reach the end of their useful life, ensuring environmental protection throughout their entire lifecycle.

Data availability

No primary research results, software or code have been included and no new data were generated or analysed as part of this review.

Author contributions

Y. W. Yang and Z. L. Huang contributed to writing – original draft. H. Gao contributed to conceptualization, project administration, funding acquisition. All authors contributed to writing – review & editing and gave approval to the final version of the manuscript.

Conflicts of interest

There are no conflicts to declare.

Acknowledgements

This study was supported by funding from the National Natural Science Foundation of China (12364014, 62041405), the Key R&D Program of Jiangxi Province, China (Grant No. 20232BBE50032), the Natural Science Foundation of Jiangxi Province, China (Grant No. 20232BAB201035, 20202BAB202011), the Education Bureau of Jiangxi Province, China (Grant No. GJJ2201028, GJJ2201003), Jingdezhen Science and Technology Plan Project (Grant No. 20212GYZD009-14, 20224GY008-02).

References

1 R. Gross, M. Leach and A. Bauen, *Environ. Int.*, 2003, **29**, 105–122.
2 P. Moriarty and D. Honnery, *Renewable Sustainable Energy Rev.*, 2012, **16**, 244–252.
3 X. Zhu, D. Yang, R. Yang, B. Yang, Z. Yang, X. Ren, J. Zhang, J. Niu, J. Feng and S. F. Liu, *Nanoscale*, 2017, **9**, 12316–12323.
4 H. Pan, X. Zhao, X. Gong, H. Li, N. H. Ladi, X. L. Zhang, W. Huang, S. Ahmad, L. Ding and Y. Shen, *Mater. Horiz.*, 2020, **7**, 2276–2291.
5 A. Kojima, K. Teshima, Y. Shirai and T. Miyasaka, *J. Am. Chem. Soc.*, 2009, **131**, 6050–6051.
6 M. Alla, V. Manjunath, N. Chawki, D. Singh, S. C. Yadav, M. Rouchdi and F. Boubker, *Opt. Mater.*, 2022, **124**, 112044.
7 T. A. Chowdhury, M. a. B. Zafar, M. S.-U. Islam, M. Shahinuzzaman, M. A. Islam and M. U. Khandaker, *RSC Adv.*, 2023, **13**, 1787–1810.
8 S. K. Sahoo, B. Manoharan and N. Sivakumar, *Stability of perovskite solar cells: issues and prospects*, Elsevier, 2018, pp. 1–24.
9 P. Zhang, M. Li and W.-C. Chen, *Front. Chem.*, 2022, **10**, 802890.
10 K. Liao, C. Li, L. Xie, Y. Yuan, S. Wang, Z. Cao, L. Ding and F. Hao, *Nano-Micro Lett.*, 2020, **12**, 1–22.
11 H. Sun, P. Dai, X. Li, J. Ning, S. Wang and Y. Qi, *J. Energy Chem.*, 2021, **60**, 300–333.
12 K. Domanski, E. A. Alharbi, A. Hagfeldt, M. Grätzel and W. Tress, *Nat. Energy*, 2018, **3**, 61–67.
13 Z. Liu, L. KrüCkemeier, B. Krogmeier, B. Klingebiel, J. A. Márquez, S. Levcenko, S. ÖZ, S. Mathur, U. Rau and T. Unold, *ACS Energy Lett.*, 2018, **4**, 110–117.
14 S. S. Mali, H. Kim, D. H. Kim and C. Kook Hong, *ChemistrySelect*, 2017, **2**, 1578–1585.
15 M. Konstantakou, D. Perganti, P. Falaras and T. Stergiopoulos, *Crystals*, 2017, **7**, 291.
16 S. Tian, J. Li, S. Li, T. Bu, Y. Mo, S. Wang, W. Li and F. Huang, *Sol. Energy*, 2019, **183**, 386–391.
17 N. a. N. Ouedraogo, G. O. Odunmbaku, Y. Ouyang, X. Xiong, B. Guo, S. Chen, S. Lu and K. Sun, *Renewable Sustainable Energy Rev.*, 2024, **192**, 114161.
18 M. Jung, S.-G. Ji, G. Kim and S. I. Seok, *Chem. Soc. Rev.*, 2019, **48**, 2011–2038.
19 H. Li, Y. Xia, C. Wang, G. Wang, Y. Chen, L. Guo, D. Luo and S. Wen, *ACS Appl. Mater. Interfaces*, 2019, **11**, 34989–34996.
20 Y. Lili, G. Yanbo, X. Yanjie, F. Xue, Y. Wang and L. Yingrui, *ACS Appl. Mater. Interfaces*, 2019, **11**, 792–801.
21 M. Xiao, F. Huang, W. Huang, Y. Dkhissi, Y. Zhu, J. Etheridge, A. Gray-Weale, U. Bach, Y. B. Cheng and L. Spiccia, *Angew. Chem., Int. Ed.*, 2014, **126**, 10056–10061.
22 H. Yang, H. Wang and J. Zhang, *Coatings*, 2019, **9**, 766.
23 Y. K. Ren, X. H. Ding, Y. H. Wu, J. Zhu and S. Dai, *J. Mater. Chem. A*, 2017, **5**, 20327–20333.
24 E. Maleki, M. Ranjbar and S. Kahani, *Prog. Color, Color. Coat.*, 2021, **14**, 47–54.
25 J. Li, R. Yang, L. Que, Y. Wang, F. Wang, J. Wu and S. Li, *J. Mater. Res.*, 2019, **34**, 2416–2424.
26 K.-M. Lee, C.-J. Lin, B.-Y. Liou, S.-M. Yu, C.-C. Hsu, V. Suryanarayanan and M.-C. Wu, *Sol. Energy Mater. Sol. Cells*, 2017, **172**, 368–375.
27 B. Gao and J. Meng, *Sol. Energy*, 2020, **211**, 1223–1229.
28 B. Gao and J. Meng, *ACS Appl. Energy Mater.*, 2020, **3**, 8249–8256.
29 B. Gao and J. Meng, *Appl. Surf. Sci.*, 2020, **530**, 147240.
30 A. D. Taylor, Q. Sun, K. P. Goetz, Q. An, T. Schramm, Y. Hofstetter, M. Litterst, F. Paulus and Y. Vaynzof, *Nat. Commun.*, 2021, **12**, 1878.
31 K. Liu, Y. Luo, Y. Jin, T. Liu, Y. Liang, L. Yang, P. Song, Z. Liu, C. Tian and L. Xie, *Nat. Commun.*, 2022, **13**, 4891.
32 Y. Liang, P. Song, H. Tian, C. Tian, W. Tian, Z. Nan, Y. Cai, P. Yang, C. Sun and J. Chen, *Adv. Funct. Mater.*, 2022, **32**, 2110139.
33 Q. Cao, T. Wang, J. Yang, Y. Zhang, Y. Li, X. Pu, J. Zhao, H. Chen, X. Li and I. Tojiboyev, *Adv. Funct. Mater.*, 2022, **32**, 2201036.

34 S. K. Podapangi, F. Jafarzadeh, S. Mattiello, T. B. Korukonda, A. Singh, L. Beverina and T. M. Brown, *RSC Adv.*, 2023, **13**, 18165–18206.
35 H. J. Kim, Y. J. Kim, G. S. Han and H. S. Jung, *Sol. RRL*, 2024, **8**, 2300910.
36 C. Dong, X. Han, Y. Zhao, J. Li, L. Chang and W. Zhao, *Sol. RRL*, 2018, **2**, 1800139.
37 D. S. Ahmed, B. K. Mohammed and M. K. Mohammed, *J. Mater. Sci.*, 2021, **56**, 15205–15214.
38 C. Fei, B. Li, R. Zhang, H. Fu, J. Tian and G. Cao, *Adv. Energy Mater.*, 2017, **7**, 1602017.
39 J. Li, X. Hua, F. Gao, X. Ren, C. Zhang, Y. Han, Y. Li, B. Shi and S. F. Liu, *J. Energy Chem.*, 2022, **66**, 1–8.
40 J. Liu, N. Li, J. Jia, J. Dong, Z. Qiu, S. Iqbal and B. Cao, *Sol. Energy*, 2019, **181**, 285–292.
41 M. K. Mohammed, S. Singh, A. K. Al-Mousoi, R. Pandey, J. Madan, D. Dastan and G. Ravi, *RSC Adv.*, 2022, **12**, 32611–32618.
42 L. Qiu, L. Dong, D. Mei, W.-H. Chen, L. Song, J. Wang, J. Zou, P.-C. Jiang, P. Du and J. Xiong, *J. Mater. Chem. C*, 2020, **8**, 12560–12567.
43 B. Gao and J. Meng, Research Square [Preprint], 2021, DOI: **10.21203/rs.3.rs-803552/v1**.
44 S.-H. Turren-Cruz, A. Hagfeldt and M. Saliba, *Science*, 2018, **362**, 449–453.
45 Q. Han, S. H. Bae, P. Sun, Y. T. Hsieh, Y. Yang, Y. S. Rim, H. Zhao, Q. Chen, W. Shi and G. Li, *Adv. Mater.*, 2016, **28**, 2253–2258.
46 J.-P. Correa-Baena, A. Abate, M. Saliba, W. Tress, T. J. Jacobsson, M. Grätzel and A. Hagfeldt, *Energy Environ. Sci.*, 2017, **10**, 710–727.
47 M. Kim, J. Jeong, H. Lu, T. K. Lee, F. T. Eickemeyer, Y. Liu, I. W. Choi, S. J. Choi, Y. Jo and H.-B. Kim, *Science*, 2022, **375**, 302–306.
48 Y. Yun, F. Wang, H. Huang, Y. Fang, S. Liu, W. Huang, Z. Cheng, Y. Liu, Y. Cao and M. Gao, *Adv. Mater.*, 2020, **32**, 1907123.
49 M. Zhang, Z. Wang, B. Zhou, X. Jia, Q. Ma, N. Yuan, X. Zheng, J. Ding and W. H. Zhang, *Sol. RRL*, 2018, **2**, 1700213.
50 D. Prochowicz, M. M. Tavakoli, A. Solanki, T. W. Goh, K. Pandey, T. C. Sum, M. Saliba and P. Yadav, *J. Mater. Chem. A*, 2018, **6**, 14307–14314.
51 S. Shan, Y. Li, H. Wu, T. Chen, B. Niu, Y. Zhang, D. Wang, C. Kan, X. Yu and L. Zuo, *SusMat*, 2021, **1**, 537–544.
52 M. Yavari, M. Mazloum-Ardakani, S. Gholipour, M. M. Tavakoli, S. H. Turren-Cruz, N. Taghavinia, M. Grätzel, A. Hagfeldt and M. Saliba, *Adv. Energy Mater.*, 2018, **8**, 1800177.
53 Y. Li, J. Shi, J. Zheng, J. Bing, J. Yuan, Y. Cho, S. Tang, M. Zhang, Y. Yao and C. F. J. Lau, *Adv. Sci.*, 2020, **7**, 1903368.
54 W. Xu, Y. Gao, W. Ming, F. He and G. Wei, *Adv. Mater.*, 2020, **32**, 2003965.
55 Z. Zhang, Y. Huang, C. Wang, Y. Jiang, J. Jin, J. Xu, Z. Li, Z. Su, Q. Zhou and J. Zhu, *Energy Environ. Sci.*, 2023, **16**, 3430–3440.
56 Y. Su, J. Yang, H. Rao, Y. Zhong, W. Sheng, L. Tan and Y. Chen, *Energy Environ. Sci.*, 2023, **16**, 2177–2186.
57 J. Zhou, F. Zhao, J. Shen, Y. Zhou and J. Chu, *J. Mater. Chem. C*, 2021, **9**, 15301–15308.
58 F. Zeng, Y. Guo, W. Hu, Y. Tan and J. Du, *J. Lumin.*, 2020, **223**, 117178.
59 X. Ge, X. Qu, L. He, Y. Sun, X. Guan, Z. Pang, C. Wang, L. Yang, F. Wang and F. Rosei, *J. Mater. Chem. A*, 2019, **7**, 27225–27235.
60 O. Weber, D. Ghosh, S. Gaines, P. Henry, A. Walker and M. IsIam, *Chem. Mater.*, 2018, **30**, 3768–3778.
61 S. Pang, H. Hu, J. Zhang, S. Lv and Y. Yu, *Chem. Mater.*, 2014, **26**, 1485–1491.
62 Z. A. Nan, L. Chen, Q. Liu, S. Wang, Z. Chen, S. Kang, J. Ji, Y. Tan, Y. Hui and J. Yan, *Chem*, 2021, **7**, 2513–2526.
63 W. Hui, L. Chao, H. Lu, F. Xia and W. Huang, *Science*, 2021, **371**, 1359–1364.
64 W. S. Yang, J. H. Noh, N. J. Jeon, Y. C. Kim, S. Ryu, J. Seo and S. I. Seok, *Science*, 2015, **348**, 1234.
65 J. W. Lee, Z. Dai, C. Lee, H. M. Lee, T. H. Han, N. De Marco, O. Lin, C. S. Choi, B. Dunn and J. Koh, *J. Am. Chem. Soc.*, 2018, **140**, 6317–6324.
66 M. J. Maieron, M. C. Roberts and S. Prentice-Dunn, *J. Pediatr. Psychol.*, 1996, **21**, 321–333.
67 N. J. Jeon, J. H. Noh, W. S. Yang, Y. C. Kim, S. Ryu, J. Seo and S. I. Seok, *Nature*, 2015, **517**, 476–480.
68 M. Kim, G. H. Kim, T. K. Lee, I. W. Choi and D. S. Kim, *Joule*, 2019, **3**, 2179–2192.
69 H. Min, M. Kim, S. U. Lee, H. Kim and S. I. Seok, *Science*, 2019, **366**, 749–753.
70 G. Kim, H. Min, K. S. Lee, D. Y. Lee, S. M. Yoon and S. I. Seok, *Science*, 2020, **370**, 108–112.
71 H. Lu, Y. Liu, P. Ahlawat, A. Mishra, W. R. Tress, F. T. Eickemeyer, Y. Yang, F. Fu, Z. Wang and C. E. Avalos, *Science*, 2020, **370**, DOI: **10.1126/science.abb8985**.
72 T. Du, T. J. Macdonald, R. X. Yang, M. Li, Z. Jiang, L. Mohan, W. Xu, Z. Su, X. Gao and R. Whiteley, *Adv. Mater.*, 2022, **34**, 2107850.
73 T. Bu, J. Li, H. Li, C. Tian and F. Huang, *Science*, 2021, **372**, 1327–1332.
74 F. Huang, Y. Dkhissi, W. Huang, M. Xiao, I. Benesperi, S. Rubanov, Y. Zhu, X. Lin, L. Jiang and Y. Zhou, *Nano Energy*, 2014, **10**, 10–18.
75 F. D. Huang, Y. Huang, W. Xiao, M. Benesperi, I. Rubanov, S. Zhu, Y. Lin, X. Jiang, L. Zhou, Y. Weale, A. Etheridge, J. McNeill, C. R. Caruso, R. A. Bach, U. Spiccia, L. Cheng and Y. Bing, *J. Power Sources*, 2015, **278**, 325–331.
76 S. Song, K. Choi, H. Snaith and T. Park, *J. Mater. Chem. A*, 2017, **5**, 3812–3818.
77 W. Nie, H. Tsai, R. Asadpour, J.-C. Blancon, A. J. Neukirch, G. Gupta, J. J. Crochet, M. Chhowalla, S. Tretiak and M. A. Alam, *Science*, 2015, **347**, 522–525.
78 A. Peter Amalathas, L. Landová, Z. K. HáJková, L. S. HoráK, M. Ledinsky and J. Holovský, *ACS Appl. Energy Mater.*, 2020, **3**, 12484–12493.

79 E. J. Cassella, E. L. K. Spooner, T. Thornber, M. E. O'kane, T. E. Catley, J. E. Bishop, J. A. Smith, O. S. Game and D. Lidzey, *Adv. Sci.*, 2022, **9**, 2270087.
80 C. Ge, B. Jiang, J. Zhu, P. Zhang, R. Ma, S. Yan, Z. Liu, A. Shaker, M. S. Salem and J. Luo, *Adv. Funct. Mater.*, 2024, **34**, 2400075.
81 E. J. Cassella, T. Thornber, R. D. Oliver, M. E. O'kane, E. L. Spooner, R. C. Kilbride, T. E. Catley, O. S. Game, A. J. Ramadan and D. G. Lidzey, *Sol. RRL*, 2024, **8**, 2300814.
82 C. E. Eperon, V. M. Burlakov, P. Docampo, A. Goriely and H. J. Snaith, *Adv. Funct. Mater.*, 2014, **24**, 151–157.
83 M. Xu, H. Zhang, S. Zhang, H. Zhu, H. Su, J. Liu, K. Wong, L. Liao and W. C. H. Choy, *J. Mater. Chem. A*, 2015, **3**, 14424–14430.
84 A. Dualeh, N. Tétreault, T. Moehl, P. Gao, M. K. Nazeeruddin and M. Grätzel, *Adv. Funct. Mater.*, 2014, **24**, 3250–3258.
85 M. Kim, G. H. Kim, K. S. Oh, Y. Jo, H. Yoon, K. H. Kim, H. Lee, J. Y. Kim and D. S. Kim, *ACS Nano*, 2017, **11**, 6057–6064.
86 J. Troughton, M. J. Carnie, M. L. Davies, C. Charbonneau, E. H. Jewell, D. A. Worsley and T. M. Watson, *J. Mater. Chem. A*, 2016, **4**, 3471–3476.
87 S. Sanchez, X. Hua, N. Phung, U. Steiner and A. Abate, *Adv. Energy Mater.*, 2018, **8**, 1702915.
88 P. You, G. Li, G. Tang, J. Cao and F. Yan, *Energy Environ. Sci.*, 2019, **13**, 1187–1196.
89 A. Yi, S. Chae, H. M. Luong, S. H. Lee, H. Lee, H. Yoon, D.-H. Kim, H. J. Kim and T.-Q. Nguyen, *Joule*, 2024, **8**, 2087–2104.
90 C. Wang, Y. Zhao, T. Ma, Y. An, R. He, J. Zhu, C. Chen, S. Ren, F. Fu and D. Zhao, *Nat. Energy*, 2022, **7**, 744–753.
91 D. Shen, H. Mao, Y. Li, A. Abate and M. Wei, *J. Mater. Chem. A*, 2018, **6**, 20289–20296.
92 H. Gao, M. Zhang, Z. Xu, Y. Chen, Y. Hu, Z. Yi, J. Huang and H. Zhu, *Dalton Trans.*, 2024, **53**, 136–147.
93 Q. Liu, Z. Ou, Z. Ma, Z. Huang, Y. Li, S. Hou, J. Ren, J. Peng, L. Bai and H. Yu, *Nano Energy*, 2024, **127**, 109751.
94 S. Sidhik, I. Metcalf, W. Li, T. Kodalle, C. J. Dolan, M. Khalili, J. Hou, F. Mandani, A. Torma and H. Zhang, *Science*, 2024, **384**, 1227–1235.
95 N. Yan, Y. Cao, Z. Dai, L. Jiang, Y. Yang, T. Li, L. Li, S. F. Liu, Z. Fang and J. Feng, *Energy Environ. Sci.*, 2024, **17**, 5070–5079.
96 J. Burschka, N. Pellet, S.-J. Moon, R. Humphry-Baker, P. Gao, M. K. Nazeeruddin and M. Grätzel, *Nature*, 2013, **499**, 316–319.
97 L. Yan, H. Huang, P. Cui, S. Du, Z. Lan, Y. Yang, S. Qu, X. Wang, Q. Zhang and B. Liu, *Nat. Energy*, 2023, **8**, 1158–1167.
98 H. Hu, D. Wang, Y. Zhou, J. Zhang, S. Lv, S. Pang, X. Chen, Z. Liu, N. P. Padture and G. Cui, *RSC Adv.*, 2014, **4**, 28964–28967.
99 E. Pérez-Gutiérrez, M. J. Percino, P. Santos, M. Ceron, P. Ceballos, D. M. Montoya, O. Barbosa-García and S. Thamotharan, *Mater. Today Commun.*, 2020, **25**, 101384.
100 J. Liu, B. Shi, Q. Xu, Y. Li, B. Chen, Q. Wang, P. Wang, Y. Zhao and X. Zhang, *Sol. Energy Mater. Sol. Cells*, 2021, **233**, 111382.